



Is oxygen storage in three-way catalysts an equilibrium controlled process?

Roman Möller^a, Martin Votsmeier^{b,*}, Christopher Onder^a, Lino Guzzella^a, Jürgen Gieshoff^b

^a Department of Mechanical and Process Engineering ETH Zurich, 8092 Zurich, Switzerland

^b Umicore AG & Co. KG, Rodenbacher Chaussee 4, 63403 Hanau, Germany

ARTICLE INFO

Article history:

Received 9 March 2009

Received in revised form 27 April 2009

Accepted 1 May 2009

Available online 9 May 2009

Keywords:

Ceria

Three-way catalyst

Oxygen storage

Simulation

Reaction mechanism

ABSTRACT

Existing reaction mechanisms for three-way catalysts ignore the oxidation of Ce_2O_3 by H_2O or CO_2 and therefore treat oxygen storage on ceria as a kinetically controlled non-equilibrium process. Such mechanisms do not correctly reproduce a number of practically important phenomena.

Based on transient concentration step experiments, this paper demonstrates that the oxidation of reduced ceria by H_2O or CO_2 plays an important role for the understanding of the oxygen storage dynamics. The results of the step experiments are well reproduced by a simple three-reaction kinetic model that takes into account the equilibrium character of oxygen storage.

There are a number of effects that cannot be understood based on the conventional non-equilibrium mechanisms:

- The oxygen storage capacity is lowered by the presence of H_2O and CO_2 .
- The oxygen storage capacity depends on the amplitude of the lambda-oscillations.
- Following a rich-lean step the catalyst emits CO/H_2 when there is no CO/H_2 in the inlet.
- Delayed CO/H_2 emissions in the so-called fuel cut-off scenario.
- The capability of the oxygen storage to dump lambda-oscillations, even if the average lambda is slightly rich.

All these effects are explained and quantitatively predicted by the equilibrium based oxygen storage model.

© 2009 Elsevier B.V. All rights reserved.

1. Introduction

Three-way catalysts are today's most successful exhaust after treatment system for gasoline engines. With a warmed up catalyst and at steady state conditions conversions of more than 95% are reached for the three pollutants CO, NO and HC.

Transient engine operation, such as accelerations, unavoidably causes temporary deviations from a stoichiometric exhaust composition. For this purpose three-way catalysts contain ceria compounds that act as an oxygen buffer [1]. During rich excursions ceria is reduced by CO or H_2 :



During a lean phase, the reduced ceria is reoxidized by oxygen:



In a modern vehicle the air-to-fuel ratio λ is controlled by a cascaded feedback control algorithm with one λ sensor upstream and a second sensor downstream of the catalyst. The operation of the controller and especially the behavior of the second lambda sensor are strongly influenced by the oxygen storage dynamics. For this reason a detailed understanding of the oxygen storage chemistry is necessary for the development of improved lambda control schemes and appropriately adapted catalyst formulations.

In the literature one finds a large number of kinetic models for three-way catalysts. These range from relatively simple models with a small number of global reactions [2–5] to mechanistic models based on a large number of elementary surface reactions [6–15]. Table 1 summarizes the oxygen storage related reactions for some widely used reaction mechanisms. Surprisingly, none of these mechanisms takes into account the oxidation of Ce_2O_3 by H_2O or CO_2 (the reverse reactions of reactions (1) and (2)). Therefore, existing mechanisms do not treat the reduction reactions (1) and (2) as equilibrium reactions. One exception is the mechanism by Auckenthaler et al. [12], where the oxidation of ceria by H_2O has been implemented as part of the water gas shift reaction mechanism.

* Corresponding author.

E-mail address: martin.votsmeier@eu.umicore.com (M. Votsmeier).

Nomenclature

A_{cat}	specific catalytic active surface (m^{-1})
A_{geo}	specific geometric catalyst surface (m^{-1})
A_i	pre-exponential factor of reaction i (s^{-1})
c_i	concentration of species i in the channel (mol/m^3)
c_{pg}	specific heat capacity of the gas phase ($\text{J}/(\text{kg K})$)
c_{ps}	specific heat capacity of the solid phase ($\text{J}/(\text{kg K})$)
D_{chan}	diameter of the channel (m)
D_{wc}	washcoat thickness (m)
$k_{c,i}$	mass transfer coefficient from the gas phase to the surface of the species i (m/s)
E_i	activation energy of reaction i (J/mol)
H_i	enthalpy of species i (J/mol)
k_i	reaction rate constant of reaction i (s^{-1})
K_i	equilibrium constant of reaction i
L	storage capacity per active surface (mol/m^2)
\dot{m}	mass flow (kg/s)
M_i	molar mass of species i (kg/mol)
\bar{M}	average molar mass of the mixture (kg/mol)
$\nu_{i,j}$	stoichiometric coefficient of species i in reaction j
p_{exh}	pressure in the catalyst (Pa)
r_i	reaction rate of reaction i (s^{-1})
R	universal gas constant ($\text{J}/(\text{mol K})$)
\dot{s}_t	reaction source term of species i (s^{-1})
T_g	temperature of the gas phase (K)
T_s	temperature of the solid phase (K)
x_i	concentration of species i in the washcoat (mol/m^3)
α	heat transfer coefficient from the solid to the gas phase ($\text{W}/(\text{m}^2 \text{K})$)
ε_g	volume fraction of the gas phase
ε_{wc}	washcoat porosity
λ	air-to-fuel ratio
λ_g	heat conductivity of the gas phase ($\text{W}/(\text{m K})$)
λ_s	heat conductivity of the solid phase ($\text{W}/(\text{m K})$)
ρ_g	density of the gas phase (kg/m^3)
$\psi_{\text{Ce}_2\text{O}_4}$	relative oxygen storage level on the ceria
$\sum \nu_i$	diffusion volume of species i in N^2 (cm^3/mol)

The fact that reduced ceria can be oxidized by H_2O or CO_2 is well known in the literature. Otsuko et al. [16] observed both reactions and found that H_2O oxidizes Ce_2O_3 much faster than CO_2 . The oxidation of Ce_2O_3 by CO_2 has also been reported by Sharma et al. [17]. The reaction of ceria with mixtures of $\text{H}_2/\text{H}_2\text{O}$ or CO/CO_2 has been used for the experimental determination of the ceria reduction thermodynamics [18–21]. Furthermore, the reactions of Ce_2O_3 with H_2O and CO_2 are discussed to play an important role in the processes for water gas shift, steam reforming and fuel reforming [22]. Padeste et al. studied the effect of water on the oxygen storage capacity and found that the storage capacity is reduced in the presence of water [23].

Despite the fact that the reactions of Ce_2O_3 with H_2O and CO_2 are well known in the literature, it seems that the role of these reactions for the understanding of the oxygen storage dynamics in three-way catalysts has not been sufficiently investigated. This statement is supported by the fact that these reactions are not included in the published reaction schemes.

Three-way catalysts, when exposed to dynamic operating conditions, show a number of effects that cannot be understood in

terms of the existing non-equilibrium oxygen storage reaction mechanisms:

- The observed oxygen storage capacity is lower in the presence of H_2O and CO_2 .
- The observed oxygen storage capacity depends on the CO/H_2 concentrations.
- When the catalyst is exposed to a rich-lean step the outlet remains rich for some time after the inlet has switched to lean. This means that the catalyst emits CO and H_2 when the inlet only contains H_2O and CO_2 .
- When a beforehand oxidized catalyst is subjected to a short rich pulse followed by stoichiometric operation, the catalyst emits a delayed pulse of CO/H_2 during the stoichiometric phase.
- When a catalyst is operated with an oscillating air-to-fuel ratio at slightly rich conditions the oscillations are adsorbed by the oxygen storage.

The purpose of this paper is to show that all these effects can be understood, if the equilibrium character of the oxygen storage reactions (1) and (2) is taken into account. In a first step the importance of the reverse reactions (–1) and (–2) is demonstrated in a series of pulse experiments. These experiments are used to parameterize a simple three-reaction equilibrium oxygen storage model.

In a second step the so far unexplained effects are reproduced in model-gas experiments and it is shown that all effects are explained and predicted by the equilibrium oxygen storage model.

2. Methodology

2.1. Experimental

The measurements for this investigation were performed on a model-gas test bench, where the exhaust gas is mixed from bottles and heated up to the desired temperature. The gas mixing system of the test bench is optimized to have a fast continuous λ adjustment with time constants comparable to an engine test bench. The time constant and transport delay, measured with lambda steps and a wide-range λ sensor, are both on the order of 150 ms. The experimental setup has been described in more detail in [24].

For the measurement of H_2 , O_2 , H_2O , CO_2 , and N_2 the test bench is equipped with a Pfeiffer Omnistar mass spectrometer that is optimized for fast response measurements. The five measured atomic masses can be scanned in less than 60 ms. Very thin and short capillaries reduce the time delay of the modified inlet system to approximately 80 ms. CO is measured using an Airsense Compact mass spectrometer.

The inlet concentrations are recorded using the mass flow sensor signals of the flow controllers.

The catalyst used in this investigation is a commercial three-way catalyst containing a ceria/zirconia mixed oxide oxygen storage compound. The precious metal loadings are $1 \text{ g}/\text{ft}^3$ rhodium, $8 \text{ g}/\text{ft}^3$ palladium, and $1 \text{ g}/\text{ft}^3$ platinum. The catalytically active material is coated on a cordierite monolith with a cell density of 600 cells per square inch. Measurements were performed on an aged (8 h 985 °C in air) sample with a diameter of one inch and a length of 3 in.

2.2. Numerical model

The catalytic monolith is modeled as a single one-dimensional and adiabatic channel. Radial heat and concentration gradients between different channels are neglected. The model consists of two gas phases and one solid phase. The first gas phase takes into

Table 1

Oxygen storage related reactions in different literature reaction mechanisms.

Koltsakis et al. [2–4]	$1/2O_2 + Ce_2O_3 \rightarrow Ce_2O_4$ $CO + Ce_2O_4 \rightarrow Ce_2O_3 + CO_2$ $H_2 + Ce_2O_4 \rightarrow Ce_2O_3 + H_2O$	5 global reactions
Hoebink et al. [6], Koci et al. [7,8] and Hayes et al. [9]	$O_2 + Ce_2O_3 \rightarrow Ce_2O_3-O_2$ $Ce_2O_3-O_2 + Ce_2O_3 \rightarrow 2Ce_2O_4$ $PtCO + Ce_2O_4 \rightarrow CO_2 + Pt + Ce_2O_3$	23 elementary reactions
Rajasree et al. [10]	$O_2 + Ce_2O_3 \rightarrow Ce_2O_3-O_2$ $Ce_2O_3-O_2 + Ce_2O_3 \rightarrow 2Ce_2O_4$ $H_2O + Ce_2O_3 \rightarrow Ce_2O_3-H_2O$ $Ce_2O_3-H_2O + Ce_2O_4 \rightarrow 2Ce_2O_3-OH$ $2Ce_2O_3-OH \rightarrow Ce_2O_3-H_2O + Ce_2O_4$ $2Ce_2O_3-H + Ce_2O_4 \rightarrow Ce_2O_3-H_2O + 2Ce_2O_3$ $Ce_2O_3-H_2O \rightarrow H_2O + Ce_2O_3$ $PtCO + Ce_2O_3-OH \rightarrow CO_2 + Ce_2O_3-H + Pt$ $PtCO + Ce_2O_4 \rightarrow CO_2 + Pt + Ce_2O_3$	17 elementary reactions
Balenovic [11]	$PtO + Ce_2O_3-CO \rightarrow CO_2 + Ce_2O_3 + Pt$ $Pt + Ce_2O_3-CO \rightarrow PtCO + Ce_2O_3$ $O_2 + 2Ce_2O_3 \rightarrow 2Ce_2O_4$ $PtCO + Ce_2O_4 \rightarrow CO_2 + Ce_2O_3 + Pt$ $PtCO + Ce_2O_3 \rightarrow Ce_2O_3-CO + Pt$ and additional reactions of ceria with ceria in the bulk	39 elementary reactions
Auckenthaler et al. [12]	$1/2O_2 + Ce_2O_3 \rightarrow Ce_2O_4$ $H_2O + Ce_2O_3 + 2Pt \rightarrow Ce_2O_4 + 2PtH$ $CO + Ce_2O_4 \rightarrow Ce_2O_3 + CO_2$ $H_2 + Ce_2O_4 \rightarrow Ce_2O_3 + H_2O$	15 elementary reactions
Chatterjee et al. [13]	–	44 elementary reactions
Kwon et al. [14]	–	24 elementary reactions
Brinkmeier et al. [15]	Integration of the deviation from stoichiometric air-to-fuel ratio	15 reactions

account the convective mass flow and heat transfer in the axial direction. The second gas phase includes the washcoat and the boundary layer close to the washcoat. Concentration gradients inside the washcoat are neglected. The mass exchange between the two gas phases is taken into account by a mass transport coefficient. Axial diffusion in the channel is neglected.

Mass balances of the gas phase in the channel:

$$\frac{\partial c_i}{\partial t} = - \frac{R}{A_{cs} p_{exh} \bar{M}} \dot{m}(z) \left(T_g \frac{\partial c_i}{\partial z} + c_i \frac{\partial T_g}{\partial z} \right) - k_{c,i} \frac{A_{geo}}{\varepsilon_g} (c_i - x_i) \quad (4)$$

Mass balances in the washcoat/wall film:

$$\frac{\partial x_i}{\partial t} = \frac{D_{chan}}{4D_{wc}\varepsilon_{wc}} \left(k_{c,i} \frac{A_{geo}}{\varepsilon_g} (c_i - x_i) + \frac{A_{cat}}{\varepsilon_g} L \dot{s}_i \right) \quad (5)$$

The mass transfer coefficient $k_{c,i}$ is calculated using the following correlation:

$$k_{c,i} = \frac{Sh_D D_{i,N_2}}{D_{chan}} \quad (6)$$

For the Sherwood number Sh_D a value of 2.47 is assumed. The binary diffusion coefficient D_{i,N_2} of the species i in N_2 is calculated as proposed by Fuller et al., see [25]. The transient terms for concentration and temperature in the gas phase (Eqs. (4) and (8)) as well as gas concentrations in the washcoat (Eq. (5)) can be deactivated in our simulator so that steady state for the corresponding species or temperature is assumed. It has been verified that for the conditions studied in this paper deactivation of the transient terms does not have any influence on the simulation results.

The energy balances are divided into a gas phase and a solid phase. Reaction heat is released only to the solid phase. Heat losses to the ambient are neglected.

The heat transfer coefficient α for the heat transfer between the gas phase and the solid phase is estimated using the following Nusselt correlation:

$$Nu_D = 2.47 = \frac{\alpha D_{chan}}{\lambda_g} \quad (7)$$

Energy balance gas phase:

$$\frac{\partial T_g}{\partial t} = - \frac{\dot{m}(z)}{A_{cs} \varepsilon_g \rho_g} \frac{\partial T_g}{\partial z} + \frac{\alpha A_{geo}}{\rho_g \varepsilon_g c_{pg}} (T_s - T_g) \quad (8)$$

Energy balance solid phase:

$$\frac{\partial T_s}{\partial t} = - \frac{\lambda_s}{\rho_s c_{ps}} \frac{\partial^2 T_s}{\partial z^2} - \frac{\alpha A_{geo}}{\rho_s (1 - \varepsilon_g) c_{ps}} (T_s - T_g) - \underbrace{\frac{A_{cat}}{\rho_s (1 - \varepsilon_g) c_{ps}} \sum_i \Delta H_i L \dot{s}_i}_{\text{reaction heat}} \quad (9)$$

The mass balance of the oxygen storage on the catalyst surface is directly calculated from the corresponding reaction source term:

$$\frac{\partial \Psi_{Ce_2O_4}}{\partial t} = \dot{s}_{Ce_2O_4} \quad (10)$$

The reaction source term \dot{s}_i of species i is calculated using the stoichiometric coefficients $\nu_{i,j}$ of species i in reaction j :

$$\dot{s}_i = \sum_j \nu_{i,j} (r_j^f - r_j^b) \quad (11)$$

The reaction rates r_{1-3} are defined as described in Section 3.2. For the reaction rate constant k_i^f an Arrhenius equation is used:

$$k_i^f = A_i e^{-E_i/RT} \quad (12)$$

The reaction rate constant of the reverse reactions is then computed from chemical equilibrium:

$$k_i^b = \frac{k_i^f}{K_i} \quad (13)$$

To ensure thermodynamic consistency of the complete mechanism all reactions are simulated as reversible reactions. The equilibrium constant K_i is calculated based on the change of the Gibbs free energy over the reaction:

$$K_i = e^{-\Delta G_i/RT} \quad (14)$$

The Gibbs free energy is defined as

$$\Delta G_i = \Delta H_i - T\Delta S_i, \quad (15)$$

where ΔS_i and ΔH_i are the entropy change and enthalpy change of the reaction. The temperature dependent enthalpies and entropies of the gas species are obtained using the program GASEQ [26]. The oxidation enthalpy of reduced ceria as a function of the degree of oxidation $\psi_{\text{Ce}_2\text{O}_4}$ is described by a second order polynomial. A constant value, independent of the degree of oxidation, is assumed for the oxidation entropy of reduced ceria. The ceria oxidation entropy, the polynomial coefficients for the ceria oxidation enthalpy, and the kinetic parameters are determined by fitting the model to experimental data (see Section 3.2).

3. Results and discussion

3.1. Ceria oxidation by H_2O and CO_2

In a first step the oxidation of Ce_2O_3 by $\text{H}_2\text{O}/\text{CO}_2$ is studied in simple pulse experiments with H_2O or CO_2 as the only oxidizing species. Fig. 1 shows results for the oxidation by H_2O . In this experiment H_2 is added periodically to the feed gas every 60 s. Fig. 1 shows one such cycle. In a first phase (10–40 s) the catalyst is reduced by a mixture of 3200 ppm H_2 and 10% H_2O . In a second phase (40–70 s) hydrogen is switched off so that the catalyst is reoxidized by H_2O . A consumption of H_2O and corresponding formation of H_2 are observed after switching off the H_2 feed. This is clear evidence that reaction (2) takes place under typical automotive exhaust conditions. When the H_2 inlet is switched on again (10 s) CeO_2 is reduced by H_2 , evidenced by a delay in the H_2 breakthrough behind catalyst. To ensure that the observed delay is not caused by the time response of the measurements the same experiment was performed without water as well. In this case the H_2 breakthrough is at 13 s instead of the delayed breakthrough at 18 s when H_2O is present.

Similar experiments have been performed for the system CO/CO_2 (Fig. 2). Again it is found that the reduced catalyst is oxidized by CO_2 (CO_2 consumption and CO formation) and the so oxidized catalyst is reduced in the following rich phase (CO formation and CO_2 consumption).

3.2. Kinetic model

To facilitate a quantitative discussion of the role of ceria oxidation by H_2O and CO_2 , a kinetic model is setup. The idea here is to present a simple model restricted to the reactants CO , H_2 , O_2 , CO_2 , and H_2O . The two main reactions considered in the model are the reversible reduction of CeO_2 by H_2 and CO . The oxidation of Ce_2O_3 by H_2O and CO_2 is taken into account by the two reverse

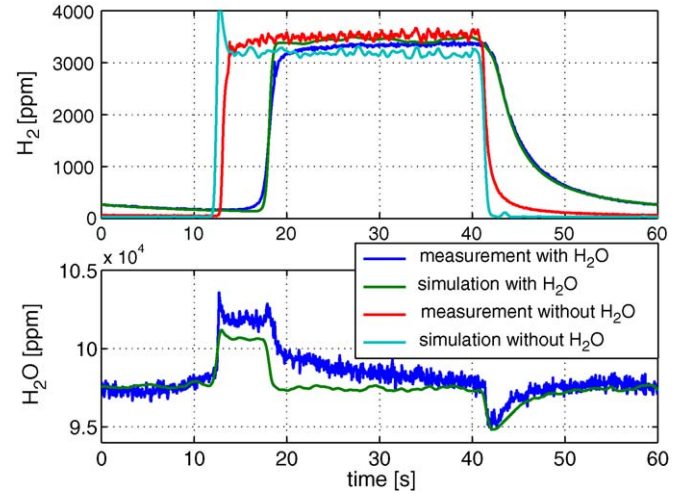


Fig. 1. Experiment that shows the oxidation of reduced ceria by H_2O . Inlet temperature = 870 K and space velocity = $78\,000\text{ h}^{-1}$. Inlet gas composition: 10% H_2O , H_2 variable, N_2 balance.

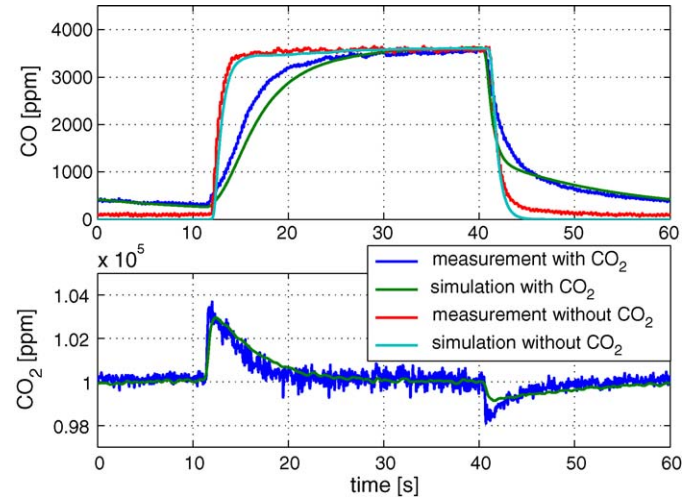


Fig. 2. Experiment that shows the oxidation of reduced ceria by CO_2 . Inlet temperature = 870 K, space velocity = $78\,000\text{ h}^{-1}$. Inlet gas composition: 10% CO_2 , CO variable, N_2 balance. For the simulation of this experiment the reaction rate of reaction (1) was lowered by a factor of 250.

reactions (–1) and (–2). Additionally the model takes into account the oxidation of Ce_2O_3 by oxygen with reaction (3).

The kinetics of the three reactions are described by the following rate laws:

$$r_1^f = k_1^f c_{\text{CO}_2} (1 - \psi_{\text{Ce}_2\text{O}_4}) \quad r_1^b = k_1^b c_{\text{CO}} \psi_{\text{Ce}_2\text{O}_4} \quad (16)$$

$$r_2^f = k_2^f c_{\text{H}_2\text{O}} (1 - \psi_{\text{Ce}_2\text{O}_4}) \quad r_2^b = k_2^b c_{\text{H}_2} \psi_{\text{Ce}_2\text{O}_4} \quad (17)$$

$$r_3^f = k_3^f c_{\text{O}_2} (1 - \psi_{\text{Ce}_2\text{O}_4})^2 \quad r_3^b = k_3^b \psi_{\text{Ce}_2\text{O}_4}^2 \quad (18)$$

The reaction orders are based on the stoichiometric coefficients of the corresponding reaction.

To estimate the kinetic parameters an experiment was performed where the temperature was slowly ramped from 600 to 200 °C (Fig. 3). During the experiment alternating pulses of CO and O_2 were periodically added to a base mixture containing 10% CO_2 , 10% H_2O (balance N_2). Fig. 4 shows results of the pulse measurements for three representative temperatures.

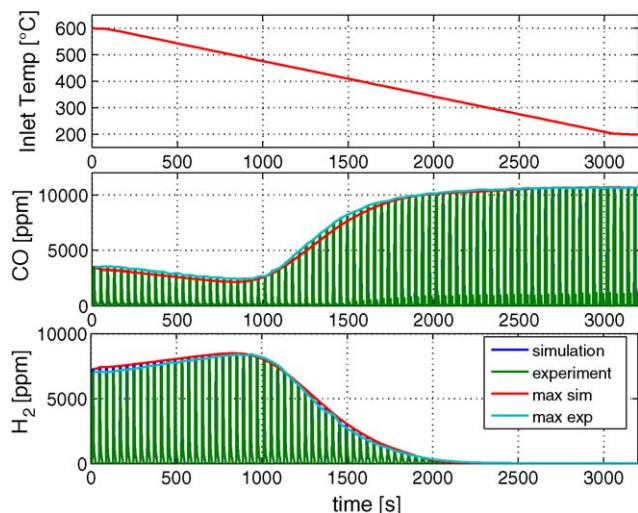


Fig. 3. Experiment used for the estimation of pre-exponential factors and the activation energies. The inlet temperature was slowly ramped from 600 °C down to 200 °C.

During the rich phases H_2 is produced from CO via the water gas shift reaction:



The resulting H_2 and CO peak concentrations during the temperature ramp are shown in Fig. 3. There is some evidence in literature that the water gas shift reaction mechanistically proceeds through a combination of reactions (1) and (–2) [27–29]. Consequently, in the current study the water gas shift reaction is not explicitly taken into account as a separate reaction. Rather, it is attempted to parameterize reaction (1) and reaction (–2) in such a

way that the combination of these two reactions correctly reproduces the steady state water gas shift reaction rates.

The kinetic parameters (pre-exponential factors A_i and activation energies E_i) of reactions (1–3) as well as the thermodynamic properties of Ce_2O_3 were fitted by a non-linear least-squares algorithm to the experimental data shown in Figs. 3 and 4. Additionally some pulse experiments with only H_2/H_2O such as the one shown in Fig. 1 and a CO/O_2 pulse sequence without H_2O and CO_2 were used for the parameter estimation.

Fig. 1, Figs. 3 and 4 compare the resulting fit to the experimental data. All data is well reproduced by the model. The estimated parameters are given in Table 2.

Fig. 5 compares the change of the Gibbs free energy ΔG for ceria oxidation obtained from our fit to data from the literature. Given the scatter in the experimental data and taking into account that the oxidation thermodynamics will depend on the exact composition of the oxygen storage material [20], the agreement with the literature values is reasonable.

It should be noted that the oxygen storage kinetics and the steady state water gas shift activity can be described by one set of kinetic parameters. This supports the assumption that the water gas shift reaction can be described by a combination of reactions (1) and (–2). It should be further noted that the same set of kinetic parameters well describes the pulse experiments with oxygen (Figs. 3 and 4) and the experiments with only H_2/H_2O (Fig. 1). This is not the case for the experiments with only CO/CO_2 . Here the experimental results show a much slower breakthrough of CO than predicted by a model that has been adapted to the pulse experiments with oxygen. The CO/CO_2 pulse experiments can be well described by the reactions (1) and (–1) if the rate constant for reaction 1 is lowered by a factor of 250. However, with this parameterization the dynamic oxygen storage behavior with oxygen and the steady state water gas shift reactivity cannot be captured. A possible explanation for the slow reaction of CO with Ce_2O_3 in the CO/CO_2 pulse experiments is catalyst deactivation by prolonged operation under rich conditions. Such a deactivation

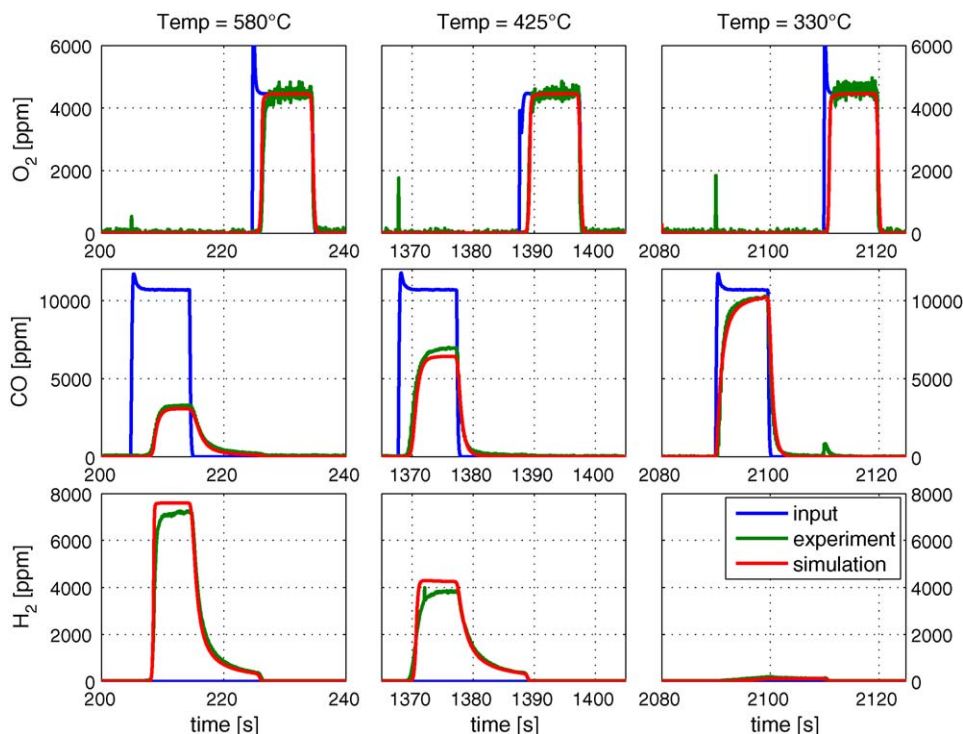


Fig. 4. Zoomed O_2 , CO and H_2 concentration transients of the experiment shown in Fig. 3 at three different times. The inlet temperatures are approximately 580 °C ($t = 220$ s), 425 °C ($t = 1380$ s) and 330 °C ($t = 2100$ s).

Table 2
Estimated parameters.

Pre-exp. factor	Activation energy	Storage capacity per catalyst volume
$A_1 = 4.10 \times 10^{14} \text{ s}^{-1}$	$E_1 = 230 \text{ kJ/mol}$	$L = 76.7 \text{ mol/m}^3$
$A_2 = 1.99 \times 10^9 \text{ s}^{-1}$	$E_2 = 160 \text{ kJ/mol}$	Entropy: $\Delta S_{\text{Ce}_2\text{O}_4} = 5 \text{ J/(mol K)}$
$A_3 = 1.61 \times 10^4 \text{ s}^{-1}$	$E_3 = 10 \text{ kJ/mol}$	Enthalpy: $\Delta H_{\text{Ce}_2\text{O}_4} = (-289 + 54\psi_{\text{Ce}_2\text{O}_4}^2) \text{ kJ/mol}$

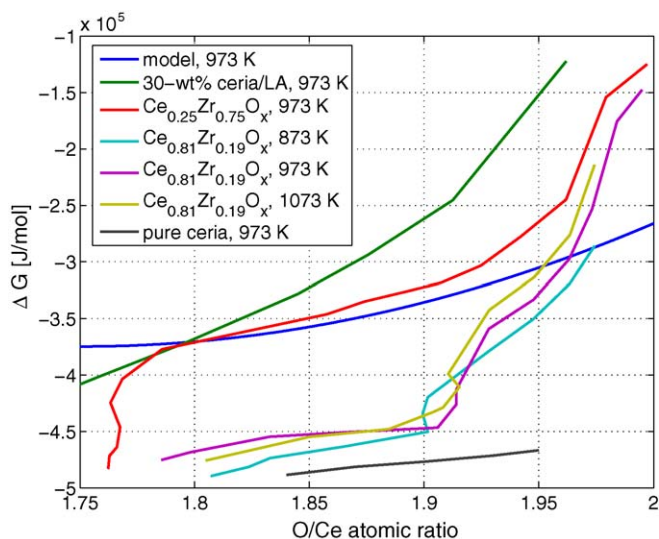


Fig. 5. Literature data and estimated values used in the model of this publication for the thermodynamic properties of ceria. Shown is the change in the Gibbs free energy of the reaction: $\text{O}_2 + 2\text{Ce}_2\text{O}_3 \leftrightarrow 2\text{CeO}_2$. Data for 30 wt.% ceria/LA is obtained from [20] and data for $\text{Ce}_y\text{Zr}_{(1-y)}\text{O}_x$ and pure ceria from [21].

phenomenon is well known in the literature [30,31] and it has been demonstrated before that a three-way catalyst needs to be operated periodically under lean conditions to avoid this deactivation [30,31]. In the CO/CO₂ pulse experiments the catalyst was continuously subjected to CO/CO₂ pulses for about 8 min. It seems that CO₂ alone is not a strong enough oxidizing agent to avoid the deactivation.

3.3. Dependency of storage capacity on exhaust composition and temperature

The oxygen storage during a rich-lean step and oxygen release in a lean-rich step are generally referred to as the catalyst's oxygen

storage capacity. This oxygen storage capacity is an important parameter for the design and calibration of the λ controller. Adaptation of the λ controller to the catalysts oxygen storage capacity is essential to reach high conversion rates under transient operating conditions. Since the oxygen storage capacity decreases over the lifetime of the catalyst, it is an important indicator for the aging level of the catalyst. Current legislation requires regular diagnosis of the catalysts aging state during vehicle operation. Most on-board diagnosis strategies measure the oxygen storage capacity and correlate this with the catalysts aging state.

Conventional models that ignore the equilibrium behavior of the ceria reduction by CO and H₂ predict that the accessible ceria is completely oxidized under lean conditions and completely reduced under rich conditions. In consequence these models predict a constant storage capacity that is independent of exhaust composition and temperature.

If the reduction of CeO₂ by CO or H₂ is assumed to be an equilibrium reaction, ceria will not be completely reduced under rich conditions but will approach an equilibrium oxidation state that is determined by the exhaust composition and temperature.

Indeed, the simple model presented in Section 3.2 predicts the following general trends:

- The storage capacity should be significantly reduced if CO₂ and H₂O are present in the exhaust.
- The storage capacity should depend on the rich amplitude.
- The storage capacity should be temperature-dependent.

To experimentally validate the effect of CO₂/H₂O on the observed storage capacity a series of λ step experiments has been performed. Fig. 6 compares results of two experiments, one measured in the presence of H₂O and CO₂, the other without H₂O or CO₂. It is evident that the presence of H₂O and CO₂ reduces the observed storage capacity to about 50% of its value without H₂O and CO₂ [23]. In both cases the experimental results are perfectly predicted by the simple three-reaction model. Automotive exhaust will always contain about 10% H₂O and CO₂. To further analyze the effect of the exhaust composition on the oxygen storage capacity in

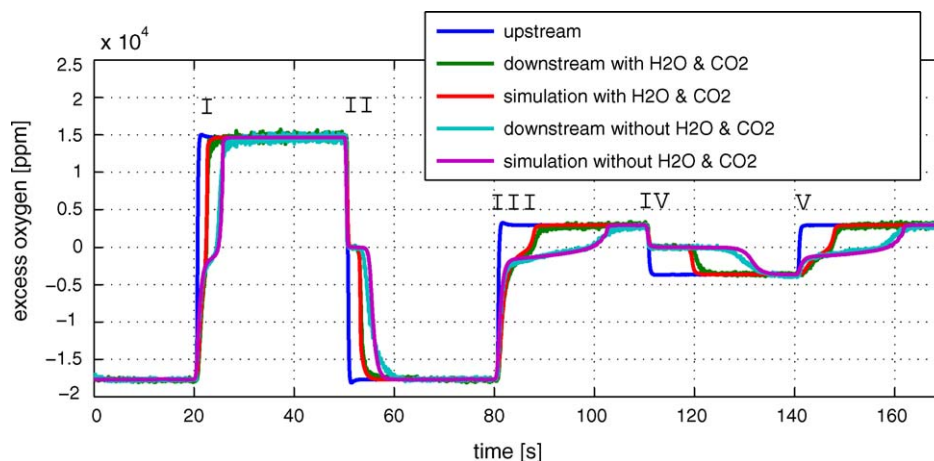


Fig. 6. Experiment showing the dependence of the oxygen storage capacity on the rich amplitude and the presence of H₂O and CO₂. The operating conditions are: inlet temperature = 870 K and space velocity = 78 000 h⁻¹. Excess oxygen = $2c_{\text{CO}_2} - c_{\text{H}_2} - c_{\text{CO}}$. Inlet gas composition: 0%/10% H₂O, 0%/10% CO₂, CO and O₂ variable, N₂ balance.

Table 3

Measured and calculated oxygen storage capacities of the experiment shown in Fig. 6.

Step no.	From λ	To λ	Capacity experiment	Capacity model
I	0.95	1.05	41.3 mol/m ³	39.1 mol/m ³
II	1.05	0.95	42.3 mol/m ³	39.0 mol/m ³
III	0.95	1.01	43.0 mol/m ³	38.8 mol/m ³
IV	1.01	0.99	31.0 mol/m ³	28.5 mol/m ³
V	0.99	1.01	29.4 mol/m ³	28.4 mol/m ³

the presence of H₂O/CO₂, an observed oxygen storage capacity has been determined for each of the λ steps in Fig. 6. For each λ step the storage capacity has been computed by numerical integration of the excess oxygen concentration. The results are shown in Table 3. It is evident that the storage capacity for the steps involving rich amplitude of 5% shows an about 30% increased storage capacity compared to the steps involving rich amplitude of 1%. Obviously the lean amplitude has no influence on the observed oxygen storage capacity. Again, the experimental results are well reproduced by the model.

3.4. Implications for three-way catalyst operation and λ control

3.4.1. Downstream air-to-fuel ratio

Most gasoline vehicles are equipped with a dual sensor λ control scheme. A first sensor measures and controls λ upstream of the catalyst, a second sensor measures λ at the catalyst outlet.

Obviously a model is only useful for the layout and calibration of such dual sensor control schemes if it correctly reproduces the downstream air-to-fuel ratio.

Fig. 7 shows measured post-catalyst λ profiles for lean-rich and rich-lean steps. The λ is calculated from the measured concentrations according to the following definition:

$$\lambda = \frac{2c_{O_2} + c_{CO} + 2c_{CO_2} + c_{H_2O}}{2c_{CO} + 2c_{CO_2} + c_{H_2} + c_{H_2O}} \quad (20)$$

In a lean-rich step the post-catalyst λ immediately assumes a value of one. This is because all the CO/H₂ in the rich inlet reacts with CeO₂. Only when the oxygen storage starts to be depleted a breakthrough of rich exhaust is observed.

Following a rich-lean step a continuous increase of the post-catalyst λ is observed. This means that for a period of about 5 s the catalyst emits rich exhaust despite the fact that the inlet contains no H₂ and only very little CO. Similar results have also been obtained in experiments where the lean phase contains no CO or H₂. This behavior cannot be reproduced by conventional models that do not take into account the equilibrium behavior of the oxygen storage.

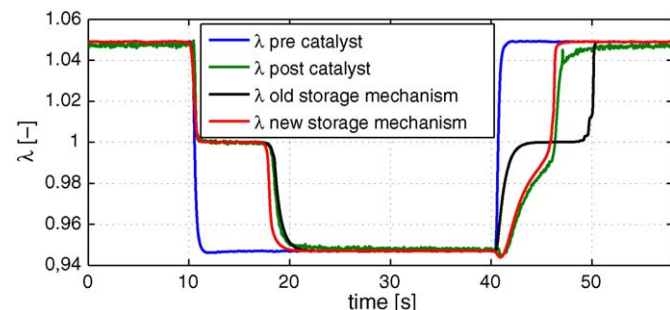


Fig. 7. Dynamic behavior of the downstream air-to-fuel ratio for the new storage mechanism compared to an existing storage mechanism. The inlet temperature = 870 K and the space velocity = 26 000 h⁻¹. Inlet gas composition: 10% H₂O, 10% CO₂, CO and O₂ variable, N₂ balance. The pre- and post-catalyst λ is calculated from measured O₂, CO, H₂, CO₂, and H₂O concentrations.

Table 4

The parameters of the non-equilibrium model.

Reaction rate constant at 870 K	Storage capacity per catalyst volume
$k_1 = 191 \text{ s}^{-1}$	$L = 42.2 \text{ mol/m}^3$
$k_2 = 45 \text{ s}^{-1}$	
$k_3 = 4030 \text{ s}^{-1}$	

To further illustrate the shortcoming of the non-equilibrium oxygen storage model such a model has been fitted to the experimental results of Fig. 7. The non-equilibrium model consists of reactions (1–3), but only takes into account the forward reactions of reactions (1) and (2). This corresponds to the conventional oxygen storage model used for example by [2]. The kinetic parameters of the non-equilibrium model are reported in Table 4. The non-equilibrium model well reproduces the lean-rich step. However, the rich-lean step is not described by the conventional model. The reason is that such a model does not contain any reactions that account for the formation of CO or H₂ so that it cannot reproduce the emission of rich exhaust under conditions where the inlet contains no CO or H₂.

The model presented in Section 3.2 accurately predicts the outlet λ during the rich-lean as well as during the lean-rich step. The rich emissions at the beginning of the rich-lean step are explained by the fact that CO and H₂ are formed by the reaction of CO₂ and H₂O with reduced ceria. This demonstrates the importance of the backward reaction paths of reactions (1) and (2).

To further analyze the relative influence of kinetic and equilibrium effects on the oxygen storage dynamics, a sensitivity study was performed where sequentially the forward and backward rates of each of the three reactions were lowered by a factor of 10. In all three cases the resulting concentration profiles showed negligible differences compared to the concentration profiles computed with the original mechanism. This proves that – at least according to the model – the oxygen storage dynamics is mainly determined by thermodynamics with only minor contributions from kinetics.

The inadequacy of current kinetic models to describe post-catalyst λ profiles has been recognized by the control engineering community and non-mechanistic empirical models have been developed that correctly reproduce post-catalyst λ profiles for certain operating conditions [32–34]. Of course, such empirical models do not convey a mechanistic understanding of the underlying chemical processes.

3.4.2. Delayed CO and H₂ emissions

During a deceleration most vehicles completely cut-off the fuel supply to the engine so that the exhaust consists of only air. Following this so-called fuel cut-off the oxygen storage of the catalyst is completely oxidized. In this situation an accidental lean excursion of the λ control will cause an immediate NO_x breakthrough. To avoid such NO_x emissions, most λ control systems apply a rich pulse after each fuel cut-off. The purpose of this rich pulse is to quickly empty the oxygen storage to its steady state operation level.

We have emulated the fuel cut-off scenario on the model-gas test bench. A typical result is shown in Fig. 8. In a first phase the catalyst is completely oxidized by a 10 s lean pulse at $\lambda = 1.1$. The lean pulse is followed by a 1 s rich pulse at $\lambda = 0.95$. Duration and amplitude of the rich pulse are chosen such that the pulse will approximately empty 20% of the ceria storage, which corresponds to approximately 40% of the storage capacity obtained with rich amplitude of 5%. After the rich pulse the inlet gas is switched to stoichiometric conditions. About 10 s after the switch to

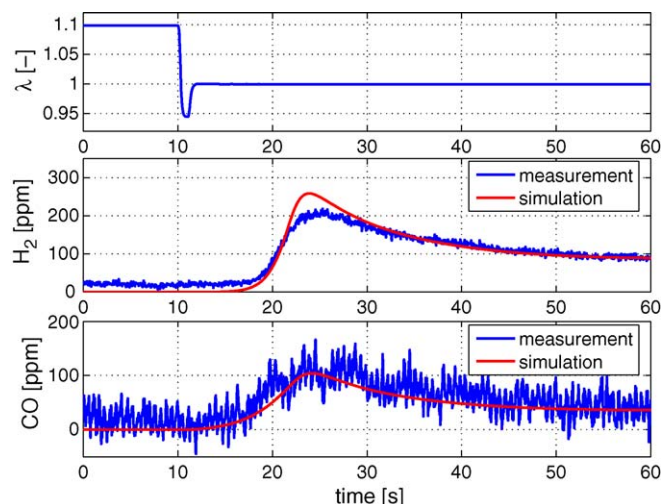


Fig. 8. Delayed emissions after a rich pulse. The inlet temperature = 770 K and the space velocity = 78 000 h⁻¹. Inlet gas composition: 10% H₂O, 10% CO₂, O₂ and CO variable, N₂ balance.

stoichiometric conditions the catalyst starts to emit CO and H₂ for about 100 s. The CO peak concentration is about 50 ppm, the H₂ peak concentration about 180 ppm. Similar rich emissions following a fuel cut-off are known to occur in vehicles.

The delayed rich emissions have important implications for current dual sensor λ control systems. In these systems the rear sensor is mounted behind the catalyst. If this sensor detects the rich emissions, the feedback control will cause the engine to run lean so that the oxygen storage is filled up. This can cause NO_x breakthroughs.

The delayed rich pulse is well predicted by the model described in Section 3.2; see Fig. 8. Fig. 9 shows computed Ce₂O₄ concentration profiles for the experiment of Fig. 8. The rich pulse reduces the oxygen storage at the inlet of the catalyst. During the stoichiometric catalyst operation the reduced zone moves downstream and after about 10 s hits the outlet of the catalyst.

3.4.3. Operation with oscillating air-to-fuel ratio

Three-way catalysts are frequently operated with an oscillating air-to-fuel ratio. In the early days of three-way catalysis the oscillations were caused by inaccuracies in the λ control. Today λ oscillations are much lower, but still present due to mass flow fluctuations and small differences between each cylinder results of

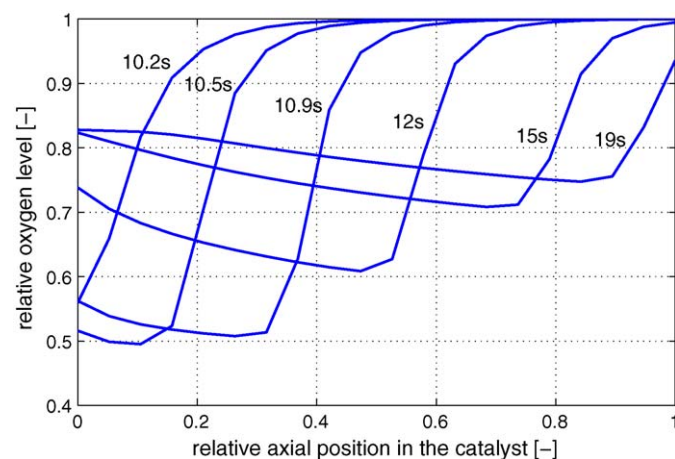


Fig. 9. Profiles of the relative oxygen filling level after the rich pulse of the experiment shown in Fig. 8. The times of the profiles are (from left to right): 10.2, 10.5, 10.9, 12, 15 and 19 s. The rich pulse starts at 10.0 s.

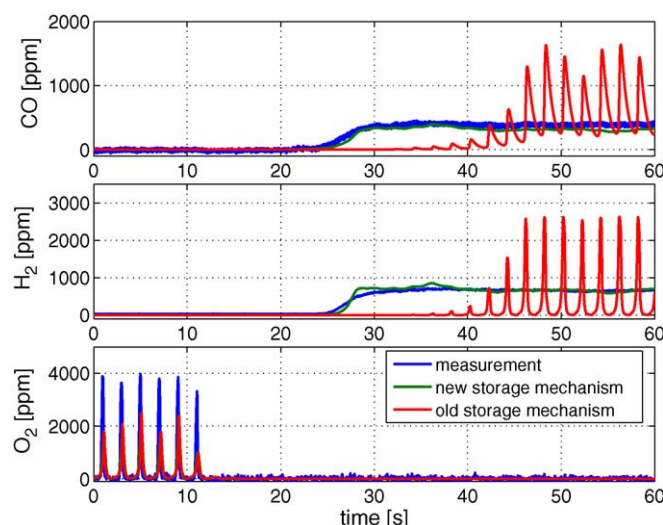


Fig. 10. Break through characteristic of emissions when a periodic excitation of the air-to-fuel ratio is applied to the catalyst. At 10 s a step from average slightly lean mixture to slightly rich was performed. The operating conditions are: inlet temperature = 870 K and space velocity = 78 000 h⁻¹. Inlet gas composition: 10% H₂O, 10% CO₂, CO/H₂ and O₂ variable, N₂ balance.

a model gas experiment which reproduces the catalyst operation with imposed lambda-oscillations. Also, many algorithms for the on board diagnosis of the catalyst's aging state use artificially imposed λ oscillations.

Fig. 10 shows results of an experiment that reproduces catalyst operation with imposed lambda-oscillations on the model gas bench. In the experiment a lambda-oscillation with a frequency of 0.5 Hz and amplitude of $\pm 3\%$ is imposed. For the first 10 s the catalysts is operated with a small lean bias of 0.3%. At 10 s a step to a rich bias of 0.3% is performed. Fig. 10 also shows the CO and H₂ outlet concentrations computed with the conventional non-equilibrium model of Section 3.4.1. During the lean phase the experimental result is qualitatively reproduced by the non-equilibrium model.

One difference between the experimental results and the output of the old model is that the model overestimates the time until the first CO/H₂ breakthrough is observed after the lean-rich step. The reason for this deviation is that the non-equilibrium model does not reproduce the dependency of the observed oxygen storage capacity on the air-to-fuel ratio. This effect has been discussed in Section 3.3. The non-equilibrium model has been calibrated in Section 3.4.1 for a step to $\lambda = 0.95$. In the experiment of Fig. 10 the rich offset is only 0.3%, leading to a significantly reduced observed storage capacity. This effect is not reproduced by the simple non-equilibrium model. Of course the storage capacity in the non-equilibrium model could be adjusted so that the model reproduces the lower observed storage of Fig. 10. However, in this case the model would not simultaneously reproduce the results of Fig. 7.

The main shortcoming of the old non-equilibrium model is that after the first rich breakthrough it predicts a continuously oscillating output. The experimental result does not show these oscillations. The reason for the oscillating output in the simple model is that due to the rich bias, the oxygen storage is completely emptied during each rich half-cycle of the oscillations. This leads to a rich breakthrough at the end of each rich half-cycle.

The equilibrium model introduced in Section 3.2 does not show the oscillating rich breakthroughs. The reason is that in the equilibrium model even under rich conditions the oxygen storage is not completely emptied, but approaches an equilibrium value. Since the equilibrium value depends on the rich amplitude, the oxygen storage can still buffer the oscillations, even if the average air-to-fuel ratio is rich.

The equilibrium model also roughly predicts the delay between the lean-rich step and the rich breakthrough. This is further evidence that the equilibrium-based model correctly reproduces the dependency of the observed storage capacity on the rich air-to-fuel ratio.

4. Conclusions

This paper demonstrates that the oxidation of Ce_2O_3 by H_2O or CO_2 plays an important role for the oxygen storage dynamics in three-way catalysts. In consequence the reduction of ceria by CO or H_2 needs to be viewed as an equilibrium process.

A set of lean-rich pulse experiments is used to parameterize a three-reaction kinetic model. This model considers the oxidation of Ce_2O_3 by O_2 and the equilibrium reactions of ceria reduction by CO and H_2 . The resulting model well describes the ceria reduction and oxidation dynamics. It also reproduces the steady state water gas shift conversion.

Existing three-way catalyst kinetic models ignore the equilibrium character of ceria reduction by H_2 or CO and consequently do not take into account the corresponding backwards reactions.

There are a number of effects that are important for the understanding of lambda control but cannot be understood based on the conventional non-equilibrium mechanisms. In this work these effects are reproduced in simple model-gas experiments. The effects are:

- The storage capacity is lower in the presence of H_2O and CO_2 .
- The storage capacity depends on the amplitude of the lambda-oscillations.
- The prolonged rich emissions following a rich-lean step.
- Delayed CO and H_2 emissions in the so-called fuel cut-off scenario.
- The capability of the oxygen storage to dump lambda-oscillations, even if the average lambda is slightly rich.

All these results are explained and quantitatively predicted by the equilibrium based oxygen storage model.

The fact that currently lambda control largely relies on heuristic control strategies may in part be related to the fact that the equilibrium character of oxygen storage dynamics has not been fully considered in previous work. It is therefore hoped that the results of this work will help to develop new and more fundamentally based lambda control and catalyst diagnosis algorithms. The ultimate goal of course will be entirely model-based control algorithms.

In the current contribution a simple three-reaction model of oxygen storage is presented. The advantage of such a simple model is that it has a limited number of parameters and therefore better supports the qualitative argumentation of this paper. For the simulation of full engine exhaust a model also covering the reactions of hydrocarbons and NO is required. A necessary next step will therefore be the implementation of an equilibrium based

oxygen storage model in a full three-way catalyst reaction mechanism.

Acknowledgements

The authors thank Thomas Bickert, Armin Wagner and Joachim Emge of Umicore for providing the experimental setup and for their help with the measurements.

References

- [1] H. Yao, Y.Y. Yau, *Journal of Catalysis* 86 (1984) 254–265.
- [2] G. Koltsakis, A. Stamatelos, *Chemical Engineering Science* 54 (1999) 4567–4578.
- [3] D. Tsinoglou, G. Koltsakis, J.P. Jones, *Industrial & Engineering Chemistry Research* 41 (2002) 1152–1165.
- [4] D. Tsinoglou, G. Koltsakis, *Chemical Engineering Science* 58 (2003) 179–192.
- [5] I. Manuel, C. Thomas, H. Colas, N. Matthes, G. Djega-Mariadassou, *Topics in Catalysis* 30/31 (2004) 311–317.
- [6] J. Hoebink, J. Harmsen, M. Balenovic, A. Back, J. Schouten, *Topics in Catalysis* 16/17 (2001) 319–327.
- [7] P. Koci, M. Kubicek, M. Marek, *Catalysis Today* 98 (2004) 345–355.
- [8] P. Koci, M. Kubicek, M. Marek, *Transactions of IChemE Part A: Chemical Engineering Research and Design* 82 (A2) (2004) 284–292.
- [9] R. Hayes, L. Mukadi, M. Votsmeier, J. Gieshoff, *Topics in Catalysis* 30/31 (2004) 411–415.
- [10] R. Rajasree, J. Hoebink, J. Schouten, *Journal of Catalysis* 223 (2004) 36–43.
- [11] M. Balenovic, *Modeling and Model-based Control of a Three-Way Catalytic Converter*. PhD thesis, Technical University of Eindhoven (2002).
- [12] T. Auckenthaler, C. Onder, H. Geering, J. Frauhammer, *Industrial & Engineering Chemistry Research* 43 (2004) 4780–4788.
- [13] D. Chatterjee, O. Deutschmann, J. Warnatz, *Faraday Discuss* 119 (2001) 371–384.
- [14] H. Kwon, J. Baik, Y. Kwon, I. Nam, S. Oh, *Chemical Engineering Science* 62 (2007) 5042–5047.
- [15] C. Brinkmeier, G. Eigenberger, S. Büchner, A. Donnerstag, *SAE Paper* 2003-01-1001 (2003).
- [16] K. Otsuka, M. Hatano, A. Morikawa, *Journal of Catalysis* 79 (1983) 493–496.
- [17] S. Sharma, S. Hilaire, J. Vohs, R. Gorte, H.-W. Jen, *Journal of Catalysis* 190 (2000) 199–204.
- [18] G. Brauer, K.A. Gingerich, U. Holtschmidt, *Journal of Inorganic & Nuclear Chemistry* 16 (1960) 77–86.
- [19] T. Kim, J.M. Vohs, R.J. Gorte, *Industrial & Engineering Chemistry Research* 45 (2006) 5561–5565.
- [20] G. Zhou, P.R. Shah, T. Montini, P. Fornasiero, R. Gorte, *Surface Science* 601 (2007) 2512–2519.
- [21] G. Zhou, P. Shah, T. Kim, P. Fornasiero, R. Gorte, *Catalysis Today* 123 (2007) 86–93.
- [22] T. Bunluesin, R. Gorte, G. Graham, *Applied Catalysis B: Environmental* 15 (1998) 107–114.
- [23] C. Padeste, N. Cant, D. Trimm, *Catalysis Letters* 18 (1993) 305–316.
- [24] R. Möller, C. Onder, L. Guzzella, M. Votsmeier, J. Gieshoff, *Applied Catalysis B: Environmental* 70 (2007) 269–275.
- [25] R. Reid, J. Prausnitz, B. Poling, *The Properties of Gases and Liquids*, 4th ed., McGraw-Hill, New York, 1986.
- [26] C. Morley, <http://www.arcl02.dsl.pipex.com>.
- [27] R. Gorte, S. Zhao, *Catalysis Today* 104 (2005) 18–24.
- [28] G. Zhou, J. Hanson, R.J. Gorte, *Applied Catalysis A: General* 335 (2008) 153–158.
- [29] S.D. Senanayake, D.R. Mullins, *Journal of Physical Chemistry C* 112 (2008) 9744–9752.
- [30] B. Campbell, R. Farrington, G. Inman, S. Dinsdale, D. Gregory, D. Eade, J. Kisenyi, *SAE Paper* 2000-01-0499 (2000).
- [31] T. Auckenthaler, *Modelling and Control of Three-Way Catalysts*, PhD thesis, Diss. ETH No. 16018. Swiss Federal Institute of Technology (ETH), Zürich, Switzerland (2005).
- [32] J.C. Peyton Jones, J.B. Roberts, P. Bernard, R.A. Jackson, *SAE Paper* 2000-01-0652 *SAE World Congress* (2000).
- [33] K. Muske, J.P. Jones, J. Howse, *Journal of Process Control* 18 (2008) 163–172.
- [34] M. Soumelidis, R. Stobart, *Proceedings of the IMechE Part I: Journal of Systems and Control Engineering* 220 (2006) 595–605.